Available online at www.sciencedirect.com
SCIENCE DIRECT®
Journal of Solid State Chemistry 178 (2005) 3315–3322
JOURNAL OF SOLID STATE CHEMISTRY
www.elsevier.com/locate/jssc

Synthesis and characterization of a Ruddlesden–Popper compound: Sr_3FeMoO_7

Zhaofei Li[a], Guobao Li[a], Junliang Sun[a], Liping You[b], Chun-K. Loong[c], Yingxia Wang[a], Fuhui Liao[a], Jianhua Lin[a,*]

[a]*State Key Laboratory of Rare Earth Materials Chemistry and Applications, College of Chemistry and Molecular Engineering, Peking University, Beijing 100871, PR China*
[b]*Electron Microscopy Laboratory, College of Physics, Peking University, Beijing 100871, PR China*
[c]*Intense Pulse Neutron Source Division, Argonne National Laboratory, Argonne, IL 60439, USA*

Received 26 April 2005; received in revised form 2 August 2005; accepted 17 August 2005
Available online 15 September 2005

Abstract

A powder sample of Sr_3FeMoO_7 was synthesized by solid-state reaction in reduced atmosphere (5% H_2/Ar). At room temperature, Sr_3FeMoO_7 crystallizes in a typical Ruddlesden–Popper ($n = 2$) structure in the space group $I4/mmm$, $a = 3.9309(2)$ Å and $c = 20.435(2)$ Å. The structure refinement indicates that the Fe and Mo ions are randomly distributed in a single *B*-site with small fraction of *B*-site and oxygen vacancies. At low temperature, long-range magnetic interaction was observed. The antiferromagnetic magnetic interaction can be described with a large unit cell, $a_m = b_m = \sqrt{2}a_n$ and $c_m = c_n$, in the magnetic space group An'.

Keywords: Sr_3FeMoO_7; Magnetic structure; Ruddlesden–Popper phase; Neutron diffraction

1. Introduction

Double perovskite Sr_2FeMoO_6 has recently aroused considerable interest due to the high Curie temperature (about 410–450 °C) and low-field magnetoresistance (MR) effect [1]. In the ordered double perovskite, Fe^{III} ($3d^5$, $S = 5/2$) is antiferromagnetically coupled to six Mo^V ($4d^1$, $S = 1/2$) neighbors resulting in effective long-range ferrimagnetic interaction. The electrons at the Fermi level are highly polarized and, the tunneling of the spin-polarized electrons through the grain boundaries leads to large negative MR effect for polycrystalline samples. In fact, the MR properties are fairly common for the double perovskite $A_2BB'O_6$, where *A* may be either alkaline earth or rare earth cations and, *B* and *B*′ are transition metal cations. For example, recent studies show that many double perovskite compounds, such as A_2FeMoO_6, A_2FeReO_6 (A = Ca, Sr, Ba) and Sr_2CrWO_6, exhibit half-metallic and MR effect [2–4]. On the other hand, the spin-polarized tunneling MR effect was also observed in single crystals of layered manganite $La_{2-2x}Sr_{1+2x}Mn_2O_7$ [5]. This layered manganite is a $n = 2$ Ruddlesden–Popper (R–P) phase and the structure can be viewed as alternative stacking of the $[MnO_6]$ double-octahedra layers and the rock salt layers. The double-octahedra layers are FM-metallic sheets and the rock salt layers act as nonmagnetic insulating barrier; thus the layered manganite crystal forms a virtually infinite array of FM/I/FM junctions. The current perpendicular to the bilayers plane carried by nearly fully spin-polarized electrons responds to magnetic field resulting in large MR effect around T_c at low field. Therefore, the R–P phases provide a nice structural model for the giant MR materials. There are a number of other compounds with R–P structures that show a MR effect, such as $Sr_3Fe_{2-x}Mn_xO_{7-\delta}$ [6], $Sr_3Fe_{2-x}Co_xO_{7-\delta}$ [7].

In comparison with the double perovskite compounds, the R–P systems with two different transition metal *B*-ions (double-T R–P phase) were less exploited. $Sr_2Mn_{0.5}Ru_{0.5}O_4$ and Sr_3MnRuO_7 are two typical examples for the double-T

*Corresponding author. Fax: +86 10 62751708.
E-mail address: jhlin@pku.edu.cn (J. Lin).

0022-4596/$ - see front matter © 2005 Published by Elsevier Inc.
doi:10.1016/j.jssc.2005.08.009

R–P compounds, in which the Mn^{IV} and Ru^{IV} are randomly distributed in the *B*-site [8]. Substituted by chemistry distinct elements, such as Li, Battle et al. [9–11] observed the local ordering at the *B*-ions within the octahedral layers, which however are randomly stacked along the *z*-axis for the $n = 1$ and 2 manganite R–P phases.

During the preparation of this paper, Cussen [12], Sher et al. [13] and Veith et al. [14] reported the syntheses and characterizations for the R–P derivative of the double perovskite Sr_2FeMoO_6, Sr_4FeMoO_8 ($n = 1$) and Sr_3FeMoO_7 ($n = 2$). They have demonstrated that the Fe^{III} and Mo^{V} ions are randomly distributed in the *B*-site in the typical R–P structures. In this paper, we will provide more experimental evidences for the structure and magnetic properties. A significant observation in our study is the long-range magnetic ordering as indicated by neutron diffraction at low temperature.

2. Experimental

Powder samples of Sr_3FeMoO_7 were synthesized at high temperature in reduced atmosphere. The stoichiometric quantities of dried $SrCO_3$, Fe_2O_3 and MoO_3 were thoroughly ground and preheated at 950 °C for 6 h in air. The obtained powders were ground and pressed into pellets of 10 mm in diameter and 2.5 mm in thickness. The pellets were sintered at 1150 °C in a flow of 5%H_2/Ar gas for 3 h and then the furnace was switched off and the sample was cooled to room temperature along with the furnace. To obtain single-phase product (which is a dark blue polycrystalline powder), intermediate grinding, pressing and heating were conducted several times to ensure the completeness of the reactions. The samples of Sr_3FeMoO_7 should be kept in desiccators.

Powder X-ray diffraction data were recorded using a Rigaku D/Max-2000 diffractometer with graphite monochromatized Cu *K*α radiation at 40 kV, 100 mA. Powder X-ray diffraction data used for structure refinement were collected in the range of 5–120° with step scanning mode with step/speed 0.02°/5 s. Electron diffraction studies were carried out on a Hitachi H-9000 electron microscope. The neutron diffraction data were measured, at 10 and 300 K using the General Purpose Power Diffractometer at the Intense Pulsed Neutron Source of Argonne National Laboratory. The resistivity measurements at different magnetic fields were performed with a PPMS 6000 (Quantum Design) using the conventional four-probe technique. The magnetization (*M*) data were measured with a commercial Quantum Design superconducting quantum interference device (SQUID) magnetometer and an Oxford MagLab-2000 magnetometer from 1.8 to 300 K. The experimental susceptibilities were corrected for the diamagnetism of the constituent atoms (Pascal's tables). The Mössbauer spectrum was obtained using ^{57}Co diffused into rhodium as a source of gamma-rays at room temperature. The XPS were acquired with a UK Kratos Axis Ultra spectrometer with Al Kα X-ray source operated at 15 kV, 15 mA. The pressure in the chamber was less than 5.0×10^{-9} Torr. Electron binding energies were calibrated against the C 1s emission at $E_b = 284.8$ eV.

3. Results

3.1. Structure refinement of Sr_3FeMoO_7 at 300 K

In Fig. 1, we show powder X-ray and neutron powder diffraction patterns for Sr_3FeMoO_7 at 300 K. Similar to previous reports [13,14], the diffraction patterns can be indexed exclusively in a typical tetragonal cell for $n = 2$ R–P in the space group $I4/mmm$, $a = 3.9310(2)$ Å and $c = 20.435(1)$ Å. This unit cell provides only a single *B*-site implying that the Fe and Mo ions are randomly distributed. To exclude the possible super-cell, which was often seen in perovskite systems, we carried out an electron diffraction study on Sr_3FeMoO_7. As shown in Fig. 2, the electron diffraction pattern in the [001] zone shows typical 4-fold symmetry without any indication for the *B*-site ordering within the *a*–*b* plane. The diffraction zone in the [100] direction also agrees with the *I*-centered tetragonal lattice. However, weak and diffusing diffraction lines can be seen along the *c*-axis (Fig. 2b), which might be an indication that the crystal contains considerable imperfections. The structure refinement was carried out with GSAS using cooperative refinement with X-ray and neutron data,

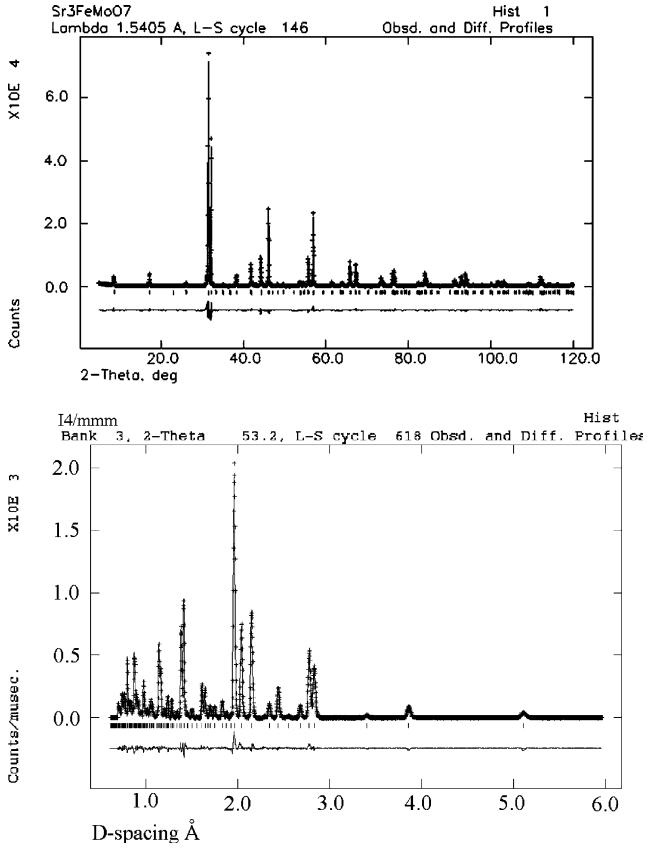

Fig. 1. X-ray and neutron powder diffraction pattern for Sr_3FeMoO_7 at 300 K.

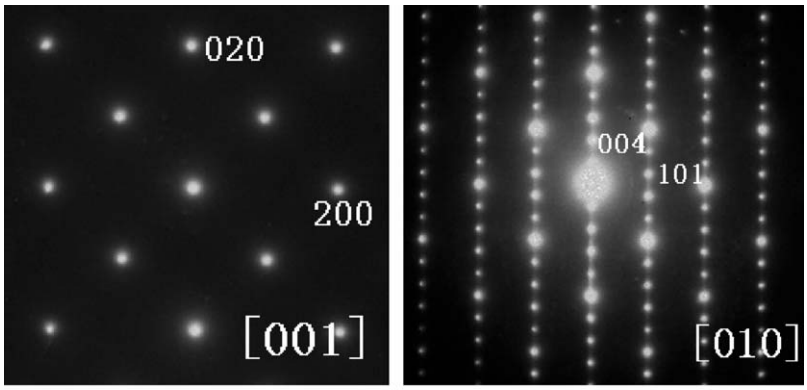

Fig. 2. Electron diffraction patterns of crystallites of Sr_3FeMoO_7 along (a) [001] and (b) [010] zone axes.

Table 1
Atomic parameters of Sr_3FeMoO_7 at 300K[a]

Atom	Site	x	y	z	U_{iso} (Å^2)	Occupation
Sr1	2*b*	0	0	1/2	0.0082(2)	1
Sr2	4*e*	0	0	0.3151(2)	0.0060(2)	1
Fe/Mo	4*e*	0	0	0.0993(2)	0.0036(1)	0.488/0.488(8)
O1	8*g*	0	1/2	0.0944(2)	0.0068(2)	1
O2	4*e*	0	0	0.1960(2)	0.0085(2)	1
O3	2*a*	0	0	0	0.0102(2)	0.904(9)
Sr1–O1		2.7540(3) × 8		Sr2–O2		2.4337(3)
Sr1–O3		2.7796(5) × 4		Fe/Mo–O1		1.9680(4) × 4
Sr2–O1		2.6980(4) × 4		Fe/Mo–O2		1.9762(6)
Sr2–O2		2.7890(3) × 4		Fe/Mo–O3		2.0300(5)

[a]Space group *I*4/*mmm* (139); $a = 3.9309(2)$ Å, $c = 20.435(2)$ Å, $V = 315.759(6)$ Å^3; $R_p = 0.041$, $R_{wp} = 0.057$; 24 variables with isotropic thermal displacement parameters.

thus balancing the scattering capacity for both metal and oxygen ions. In principle, the structure of Sr_3FeMoO_7 is an *I*-centered tetragonal $n = 2$ R–P structure similar to the previous results [13,14], in which the Fe and Mo ions are randomly distributed in a single *B*-site at room temperature. Our structure refinement indicated unambiguously the low electron density at both the Fe/Mo and the 2*a* oxygen sites, which is different from the result of Veith et al. [14] that only oxygen vacancies at the 2*a* site were observed. To accord the low electron density at the Fe/Mo site, one could consider two models either with fully occupied sites but varied Fe/Mo ratio or with fixed Fe/Mo ratio but varied occupation factor. Both models gave rise to similar fitting. However, considering the fixed Fe/Mo ratio in the syntheses, as well as the random distribution of Fe and Mo ions, the cation vacancy model at the Fe/Mo site seems more reasonable. Furthermore, the refined occupation factor at the 2*a* oxygen site accords with the cation vacancies reasonably well, which further supports the fact that both 2*a* oxygen and Fe/Mo sites are only partially occupied. As indicated [7,14], the R–P phases often contain intergrowth defects, where the octahedral layers of different thickness may form stacking fault along the *c*-axis. The electron diffraction pattern (Fig. 2b) did show weak diffusing lines, which might be an indication that the crystal consists certain intergrowth defect as suggested by Veith et al. [7,14]. However, the structure refinement of taking account only of oxygen and Fe/Mo vacancies led to a reasonable fitting; therefore, the influence of the intergrowth defect was not considered in the structure refinement. In Table 1, we list the refined structural parameters at 300 K. Selected bond lengths in Sr_3FeMoO_7 are also listed in the table.

3.2. Structure refinement of Sr_3FeMoO_7 at 10 K

In comparison with the neutron diffraction pattern at 300 K, the diffraction pattern at 10 K contains extra peaks. In Fig. 3, we compare the neutron patterns at 300 and 10 K in a high *d*-spacing range, in which additional reflection peaks at 10 K can be clearly seen. The 10 K diffraction pattern can be indexed with a larger tetragonal unit cell, $a_m = \sqrt{2}a_n$ and $c_m = c_n$, where the subscripts m and n represent magnetic and nuclear cells, respectively. In the refinement, the nuclear structure was derived directly from the room-temperature structure, while the magnetic

structure was modeled by assuming long-range antiferromagnetic interaction in the large unit cell, $a = 5.5561(3)$ Å and $c = 20.430(2)$. The magnetic space group An' was used to describe the antiferromagnetic alignment of the magnetic moments. In this magnetic space group, the *B*-site atoms split into two independent atoms. The magnetic moments of the two *B*-sites were refined independently, both in magnitude and orientation, which, however, yielded almost identical but antiparallel atomic moment, $\mu_{M1} = 1.82(1)\mu_B$ and $\mu_{M2} = 1.68(1)\mu_B$, indicating that the two *B*-sites are coupled antiferromagnetically. In addition, since the Mo and Fe ions are randomly distributed, it is not surprising that the atomic moments have the same value for the two *B*-sites. In Fig. 4, we show the Rietveld fitting of the neutron diffraction data for Sr_3FeMoO_7 at 10 K. The refined atomic and magnetic parameters are listed in Tables 2 and 3.

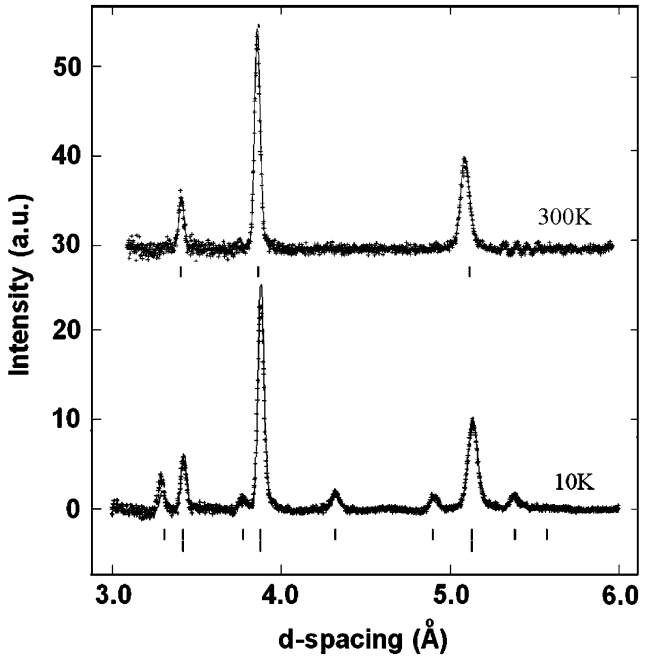

Fig. 3. Neutron powder diffraction patterns of Sr_3FeMoO_7 at 300 and 10 K in the large *d*-spacing range; the nuclear and magnetic reflections are shown below the patterns.

Fig. 5 shows the nuclear and magnetic structures of Sr_3FeMoO_7. One can see that the antiferromagnetic ordering of the neighboring *B*-ions leads to a large magnetic unit cell. The magnetic moments are not aligned along the *c*-axis but canted resulting in a lower symmetry for the magnetic structure. In the structure refinements, we assumed that the nuclear structure was retained at both room and low temperatures, i.e., the Fe^{III} and Mo^{V} ions are randomly distributed in the *B*-sites.

3.3. XPS and Mössbauer spectra

The oxidation states of the transition metal cations (Fe and Mo) in Sr_3FeMoO_7 were studied with XPS and Mössbauer spectra. Fig. 6 shows the XPS spectra for Fe and Mo in Sr_3FeMoO_7. The binding energy is about

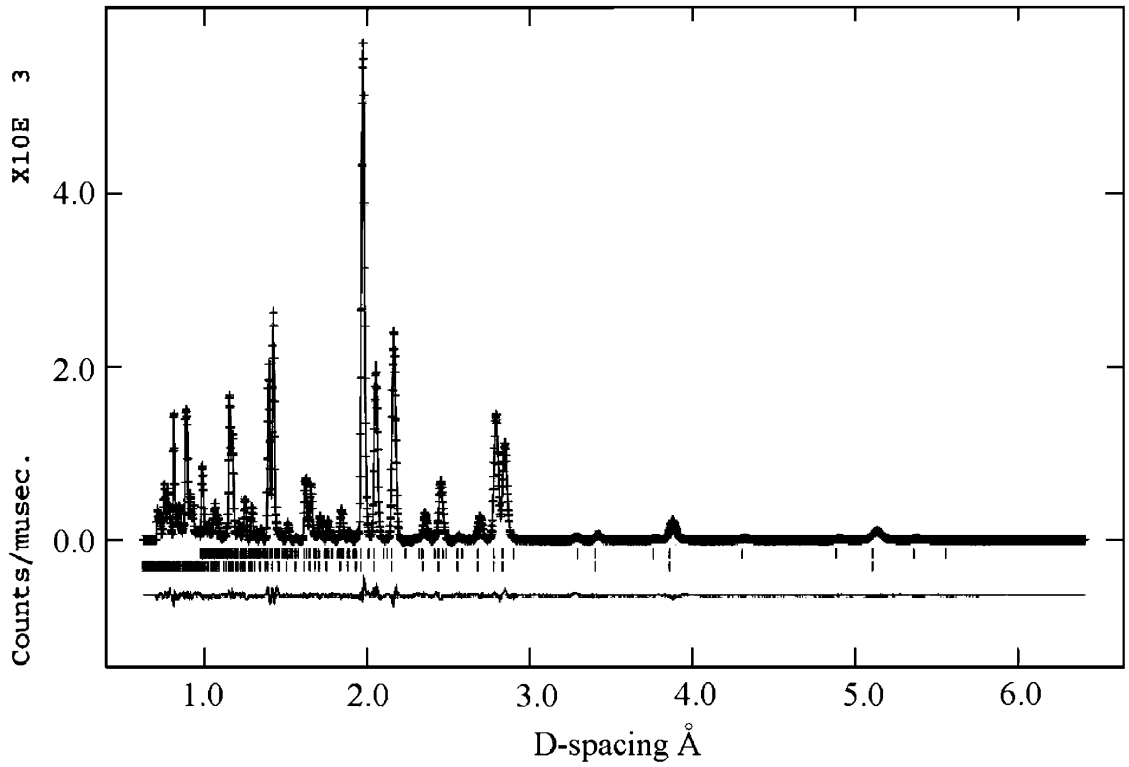

Fig. 4. Rietveld fitting for the neutron diffraction pattern of Sr_3FeMoO_7 at 10 K with the nuclear phase in space group $I4/mmm$ and magnetic phase in the magnetic space group An'.

Table 2
Atomic parameters of Sr_3FeMoO_7 at 10 K[a]

Atom	Site	x	y	z	U_{iso} (Å^2)	Occupation
Sr1	2*b*	0	0	1/2	0.0059(2)	1
Sr2	4*e*	0	0	0.3154(1)	0.0041(2)	1
Fe/Mo	4*e*	0	0	0.0995(2)	0.0040(1)	0.488/0.488
O1	8*g*	0	$\frac{1}{2}$	0.0945(2)	0.0066(2)	1
O2	4*e*	0	0	0.1966(1)	0.0072(2)	1
O3	2*a*	0	0	0	0.0094(2)	0.904
Sr1–O1		2.7539(3) × 8		Sr2–O2		2.4278(4)
Sr1–O3		2.7781(3) × 4		Fe/Mo–O1		1.9670(3) × 4
Sr2–O1		2.6926(7) × 4		Fe/Mo–O2		1.9836(5)
Sr2–O2		2.7888(5) × 4		Fe/Mo–O3		2.0318(4)

[a]Space group $I4/mmm$ (139); $a = 3.9288(2)$ Å, $c = 20.429(2)$ Å, $V = 315.346(4)$ Å^3, $R_p = 0.035$, $R_{wp} = 0.044$; 29 variables with isotropic thermal displacement parameters; the occupation factors are fixed to the values from the structure refinement at 300 K.

Table 3
Refined magnetic moments (μ_B) for Sr_3FeMoO_7 at 10 K*

Atoms	Z	Occupy	M_x	M_y	M_z	$\lvert M\rvert$
Mo/Fe1	0.9005(1)	0.488/0.488	1.30(1)	0.60(1)	1.12(1)	1.82(1)
Mo/Fe2	0.0995(1)	0.488/0.488	0.94(1)	−0.55(1)	−1.28(1)	1.68(1)

Magnetic space group: An', $a = 5.5562(3)$ Å and $c = 20.429(2)$ Å, $R_p = 0.034$, $R_{wp} = 0.046$.

710.5 eV ($2p_{2/3}$) for Fe and 232.0 eV ($3d_{5/2}$) for Mo, which agrees with the typical values of Fe^{III} and Mo^{V} in Sr_2FeMoO_6 (710.1 and 232.2 eV) [15]. The presence of Fe^{III} is further confirmed by Mössbauer spectroscopy. As shown in Fig. 7, the Mössbauer spectrum can be fitted with two components, with isomer shift $\delta = 0.48$ mm/s, quadrupole splitting $\Delta = 0.32$ mm/s and the line width $\Gamma = 0.44$ mm/s for the first and $\delta = 0.32$ mm/s, $\Delta = 0.68$ mm/s and $\Gamma = 0.42$ mm/s for the second. These two components originate from Mössbauer absorption of Fe^{III} ions. A similar Mössbauer spectrum was reported by Veith et al. [14], but they interpreted the spectrum with the three-component model. They also measured the Mössbauer spectra at low temperatures and found broad single magnetic sextet absorption at 4.2 K. The Mössbauer spectrum seems inconsistent with the random structure model since only one *B*-site is present in the structure. However, one should keep in mind that the diffraction techniques concern mainly the long-range periodicity, while Mössbauer spectroscopy is sensitive to the local coordination of the iron atoms in the structure. A possible explanation for the two absorption components in Mössbauer spectrum might be following. Assuming Fe^{III} and Mo^{V} are randomly distributed in a single *B*-site, on average each Fe octahedron would be surrounded by 2.5 Fe-octahedra and 2.5 Mo-octahedra, since each octahedron in $n = 2$ RP structure has five neighboring octahedra. Microscopically, the number of the neighboring octahedra should be an integer. Therefore, the utmost surrounding octahedra should be either 3 Fe- and 2 Mo-octahedra or 2 Fe- and 3 Mo-octahedra. These two different utmost local environmental spheres may cause the two observed major components in the Mössbauer spectrum. The other local environmental spheres, such as 4 Fe- and 1 Mo-octahedra, are also possible, but should be less preferential, particularly when thermal equilibrium has been achieved.

3.4. Magnetic and conductive measurements

Fig. 8 shows the temperature and magnetic field dependence of magnetization for Sr_3FeMoO_7. The temperature dependence of the magnetization in 0.1 T shows a complex antiferromagnetic behavior. The magnetic susceptibility increases almost linearly with the decrease of temperature. An antiferromagnetic abnormity at about 25 K was observed, which is significantly lower than 85 K observed by Veith et al. [14]. The field dependence of magnetization does not reach the saturation value up to 7 T even at 1.8 K for Sr_3FeMoO_7, which is different from that of disordered double perovskite, which reaches saturation at about 1 T. The conductivity measurement (Fig. 9a) indicates that Sr_3FeMoO_7 is an insulator but with a five-order magnitude change over the temperature range studied. The MR effect is rather small at high temperature but increases with decreasing temperature, reaching a value of ~50% at 5 K (Fig. 9b).

4. Discussion

It is well known that the ordering of transition metal ions at the *B*-site strongly influences magnetic properties for the double perovskites. One of the useful strategies to enhance

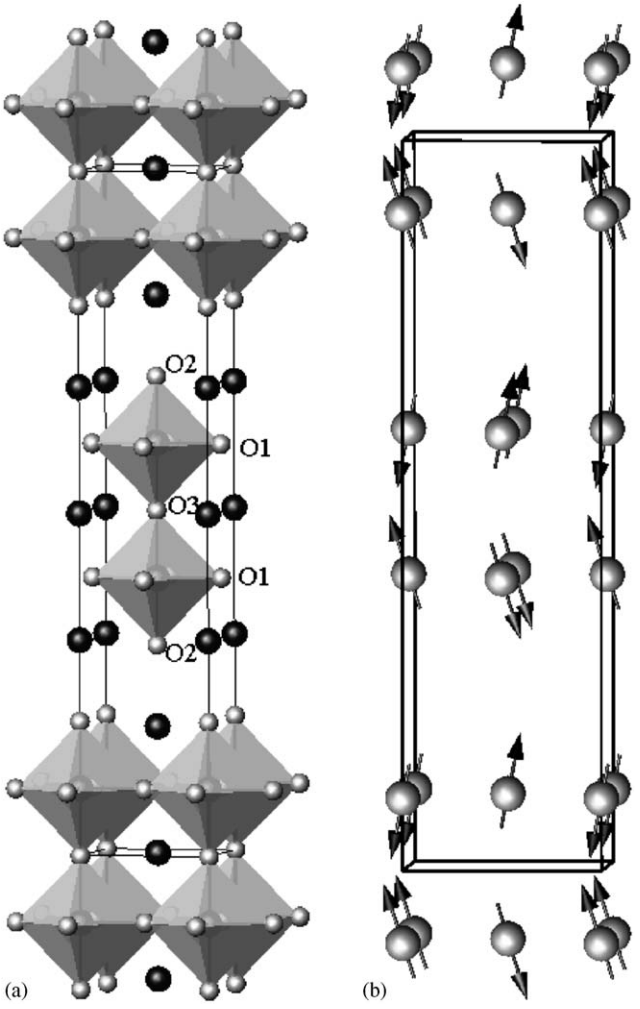

Fig. 5. Crystal structure (a) and the orientation of the magnetic moments of Sr_3FeMoO_7 at 10 K (b).

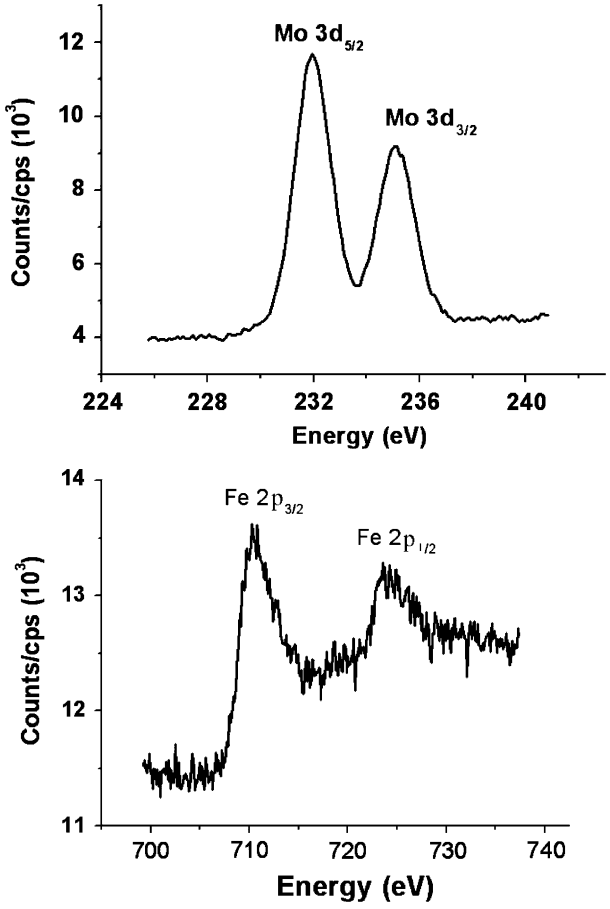

Fig. 6. XPS spectra of Mo 3*d* and Fe 2*p* in Sr_3FeMoO_7.

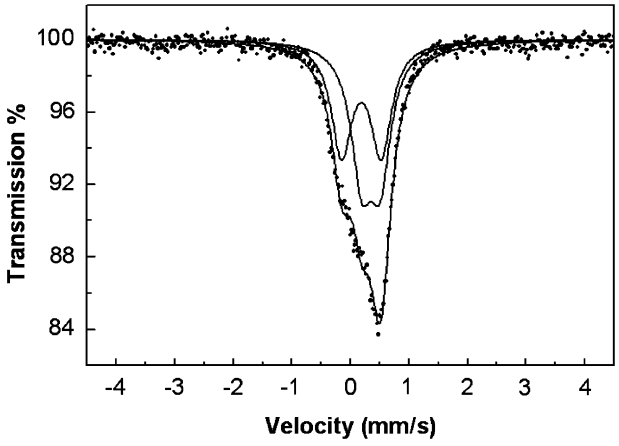

Fig. 7. Mössbauer spectrum of Sr_3FeMoO_7 at 300 K.

the *B*-site ordering is to anneal samples at certain temperatures [16]. For Sr_3FeMoO_7, we carried out annealing treatment in 5%H_2/Ar at 900 ° and 1000 °C, but no significant improvement for *B*-site ordering was achieved. The difficulty in preparing the ordered Sr_3FeMoO_7 is perhaps due to the low-dimensional structure. Battle et al. [9–11] attempted to induce the ordering at the *B*-site in the R–P phases by introducing chemically distinct element (Li^+). They did observe the local ordering at the *B*-ions within the octahedral layers in several compounds, such as in La_4LiMnO_8 and $La_3SrLiMnO_8$ [9]. However, the stacking of the octahedral layers still remained disordered along the *z*-axis. It seems that obtaining ordered R–P phases is more difficult than the corresponding double perovskite.

The magnetic interaction in Sr_3FeMoO_7 is rather complicated largely due to the random distribution of the *B*-cations. In such a system, magnetic interaction may microscopically be frustrated and thus the overall magnetic property of the material is the average of the frustration. In comparison with the results reported by Sher et al. [13] and Veith et al. [14], the overall temperature dependence curves are rather similar for magnetic susceptibility and conductivity, but our data show that the temperature of antiferromagnetic abnormity is significantly lower. In addition, our neutron diffraction data indicated undoubtedly the presence of magnetic reflections at 10 K. At present, we do not know the reason for this discrepancy, but some hints from the structure refinements should be

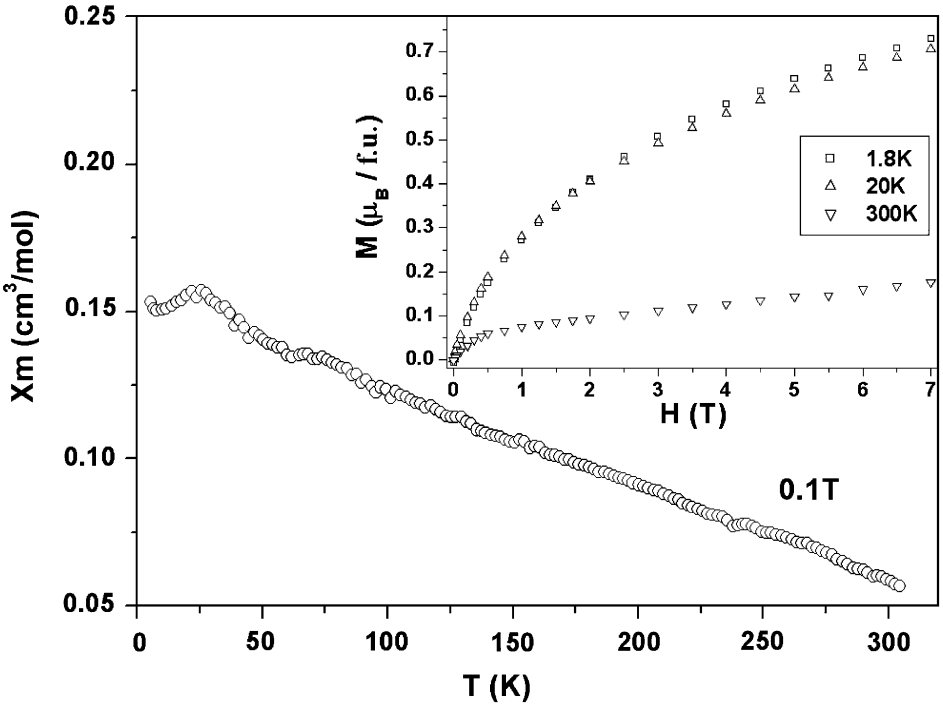

Fig. 8. Temperature dependence (0.1 T) and magnetic field (insert) dependence of the magnetization of Sr_3FeMoO_7.

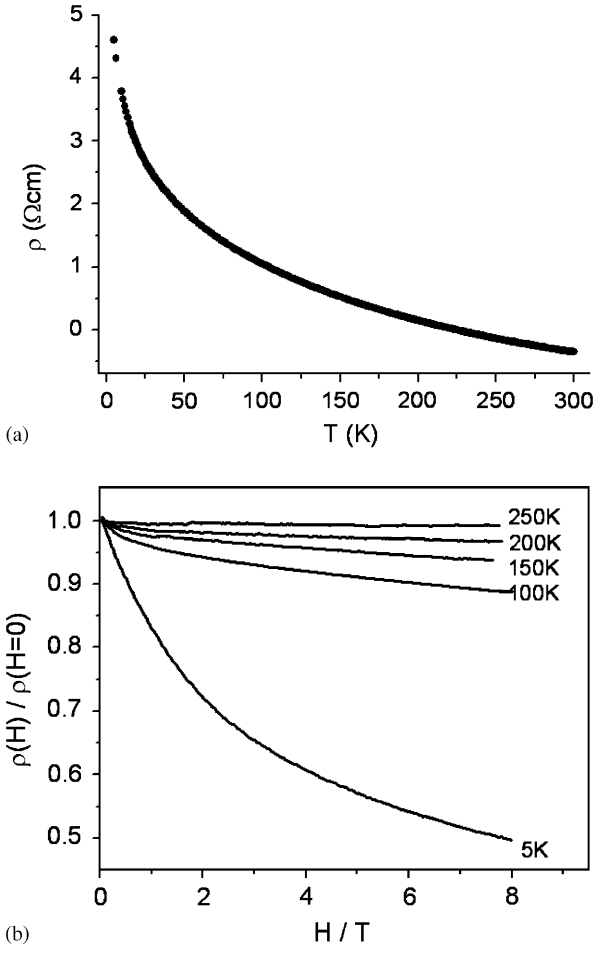

Fig. 9. Resistivity as a function of temperature (a) and magnetoresistance (b) as a function of magnetic field and temperature of Sr_3FeMoO_7.

emphasized. Our structure refinement indicated the presence of small amount of vacancies at the *B*-site and 2*a* oxygen site in Sr_3FeMoO_7. Whereas in the previous studies, no vacancies were observed in [13] and only 2*a* oxygen vacancies were reported in [14]. This means that although the basic framework of the structure may be the same, the imperfections of the crystals can be manipulated by reaction conditions, which in turn can modify the physical properties of the materials.

The Mössbauer spectrum of our sample looks rather similar to that observed by Veith et al. [14]. They interpreted the result with three components. Our data, however, could be fitted nicely by two components with almost equal intensities, which we interpreted by the two utmost distributions of the neighboring Fe- and Mo-octahedra. In addition, the magnetization at 300 K shows a nice linear dependence in the high-*H* region and therefore, it could be considered as being composed of two components, a spontaneous component reaching to saturation at low-*H* and a paramagnetic component showing a linear dependence on the magnetic field. At low temperatures (1.8 and 20 K), the linear region suppressed, while the spontaneous region expanded, which implies the presence of frustration for the magnetic interaction.

In conclusion, the neutron diffraction study confirmed that Sr_3FeMoO_7 crystallizes in typical $n = 2$ R–P structure ($I4/mmm$) at room temperature, in which the Fe^{III} and Mo^{V} ions are randomly distributed in a single octahedral site. At low temperature, the neighboring transition metal atoms are antiferromagnetically coupled leading to a large unite cell, $a_m = \sqrt{2}a$ and $c_m = c$. The neutron data at 10 K are fitted very well with an antiferromagnetic model, where

the two sites are antiferromagnetically coupled with almost the same magnetic moment $\mu_{M1} = 1.82(1)\mu_B$ and $\mu_{M2} = 1.68(1)\mu_B$. At present, considerable controversies are still left for the magnetic structures and properties of this material. One of the possible reasons for these controversies is that the magnetic interaction in Sr_3FeMoO_7 is complicated and may be manipulated by the synthetic conditions of the samples. Therefore, the conclusive magnetic structure and properties may require a more comprehensive investigation on this material.

Acknowledgments

This work was supported by the Nature Science Foundation of China (20221101 and 20371005) and by the State Key Basic Research Program of China.

References

[1] K.I. Kobayashi, T. Kimura, H. Sawada, K. Terakura, Y. Tokura, Nature 395 (1998) 677.
[2] C. Ritter, M.R. Ibarra, L. Morellón, J. Blasco, J. Garcia, J.M. De Teresa, J. Phys.: Condens. Matter 12 (2000) 8295.
[3] W. Prellier, W. Smolyaninova, A. Bisbas, C. Galley, R.L. Greene, K. Ramesha, J. Gapalakrishnan, J. Phys.: Condens. Matter 12 (2000) 965.
[4] K.-I. Kobayashi, T. Kimura, H. Sawada, K. Terakura, Y. Tokura, Phys. Rev. B 59 (1999) 11159.
[5] Y. Moritomo, A. Asamitsu, H. Kuwahara, Y. Tokura, Nature 380 (1996) 141.
[6] G.M. Veith, I.D. Fawcett, M. Greenblatt, M. Croft, I. Nowik, Int. J. Inorg. Mater. 2 (2000) 513.
[7] G.M. Veith, R. Chen, G. Popov, M. Croft, Y. Shokh, I. Nowik, M. Greenblatt, J. Solid State Chem. 166 (2002) 292.
[8] D.J. Gallon, P.D. Battle, S.J. Blundell, J.C. Burley, A.I. Coldea, E.J. Cussen, M.J. Rosseinsky, C. Steer, Chem. Mater. 14 (2002) 3976.
[9] J.C. Burley, P.D. Battle, D.J. Gallon, J. Sloan, C.P. Grey, M.J. Rosseinsky, J. Am. Chem. Soc. 124 (2002) 620.
[10] J.C. Burley, P.D. Battle, P.J. Gaskell, M.J. Rosseinsky, J. Solid State Chem. 168 (2002) 202.
[11] P.D. Battle, J.C. Burley, D.J. Gallon, C.P. Grey, J. Sloan, J. Solid State Chem. 177 (2004) 119.
[12] E.J. Cussen, M.F. Thomas, J. Mater. Chem. 15 (2005) 1084.
[13] F. Sher, A.J. Williams, A. Venimadhev, M.G. Blamire, J.P. Attfield, Chem. Mater. 17 (2005) 1792.
[14] G.M. Veith, M. Greenblatt, M. Croft, K.V. Ramanujachary, J.H. Simpers, S.E. Lofland, I. Nowik, Chem. Mater. 17 (2005) 2562.
[15] H. Falcón, J.A. Barbero, G. Araujo, M.T. Casais, M.J. Martinez-Lope, J.A. Alonso, J.L.G. Fierro, Appl. Catal. B: Environmental 53 (2004) 37.
[16] D.D. Sarma, E.V. Sampathkumaranb, S. Raya, R. Nagarajanb, S. Majumdarb, A. Kumara, G. Nalinia, T.N. Guru Rowa, Solid State Commun. 114 (2000) 465.